ISSN NO: 2770-4491
June 2026

Design and Investigation of a Novel Construction of a Horizontal-Axis Wind Energy System

Qamariddin Sayfiddinov
Bukhara State Technical University, 200100, 15 Q. Murtazoyev Street, Bukhara city, Uzbekistan
*qamariddinsayfiddinov@gmail.com

Abstract
This paper presents the design, mathematical modeling, and aerodynamic performance investigation of a novel multi-rotor counter-rotating horizontal-axis wind turbine (HAWT) system tailored for low-wind-speed operating conditions. The proposed design integrates three coaxial rotors arranged in series: two forward rotors of radii R_1 and R_2 rigidly mounted on a primary shaft driving the generator inductor, and a third rear rotor of radius R_3 mounted on an independent shaft driving the generator armature in the counter-rotating direction. This mechanical configuration doubles the relative rotational velocity within the electromechanical conversion unit without requiring a mechanical gearbox, effectively reducing mechanical losses and starting torque. A modified 1D actuator disc theoretical model incorporating sequential axial induction factors is derived using mass conservation and Bernoulli equations to quantify dynamic pressure discontinuities across the rotor stages. Aerodynamic modeling performed in Ansys Fluent demonstrates that under optimal operatinal parameters. The proposed configuration exhibits high potential for standalone micro-energy systems and off-grid decentralized power generation.

Keywords: multi-rotor wind turbine, counter-rotating system, horizontal-axis wind turbine, aerodynamic modeling, Betz limit, power coefficient, axial induction factor, CFD, Ansys Fluent.

1. Introduction

The escalating global demand for clean energy and the urgent need to mitigate greenhouse gas emissions have positioned wind power as one of the most viable and rapidly advancing renewable energy resources. While large-scale wind farms utilizing standard single-rotor horizontal-axis wind turbines (HAWTs) dominate utility-scale power grids, harvesting wind energy in low-wind-speed regimes, inland terrains, and urban environments presents substantial aerodynamic and mechanical challenges. Conventional single-rotor turbines operating under low flow velocities suffer from inadequate starting torque, significant wake rotation losses, and restricted aerodynamic efficiency governed by the classical Betz limit. To surpass the classical aerodynamic limit and extract unused kinetic energy from the rotational wake flow, multi-rotor and counter-rotating wind turbine (CRWT) architectures have garnered significant research interest [1, 2]. In a conventional single-rotor configuration, angular momentum imparted to the flow behind the rotor plane represents an irreversible energy dissipation. In contrast, dual-rotor and multi-rotor counter-rotating configurations actively recover wake swirl energy, restore rectilinear airflow downstream, and substantially increase aerodynamic power density per unit swept frontal area [3, 4]. Furthermore, by coupling dual counter-rotating shafts directly to the inductor (field winding/permanent magnets) and armature of a dedicated electrical generator, the relative rotational velocity between electromagnetic components is doubled. This allows the elimination of heavy, failure-prone mechanical step-up gearboxes, drastically reducing mechanical friction, cut-in wind speed, and capital maintenance expenditures [5]. Despite the evident aerodynamic merits of multi-rotor systems, existing investigations predominantly center around dual-rotor arrangements. Multi-stage three-rotor configurations that systematically capture kinetic energy across stepped radial zones while maintaining structural simplicity remain largely unexplored. Modeling such multi-rotor interactions requires extending momentum theory to account for aerodynamic coupling, staged induction factors, and static pressure recovery across successive rotor planes.

The aim of this study is to design a novel three-rotor counter-rotating horizontal-axis wind turbine system and analyze its aerodynamic performance under variable wind conditions. A mathematical model based on mass continuity, the momentum theorem, and Bernoulli's formulations is developed to determine the relationship between rotor radii ratios, axial induction factors, static pressure differences, and total power extraction. In addition, computational fluid dynamics (CFD) modeling in Ansys Fluent is employed to evaluate the optimum inter-rotor distance and identify the maximum achievable power coefficient (C_p).

2. Material and methods

The structural schematic and kinematic arrangement of the proposed horizontal-axis wind turbine system are depicted in **Figure 1**.

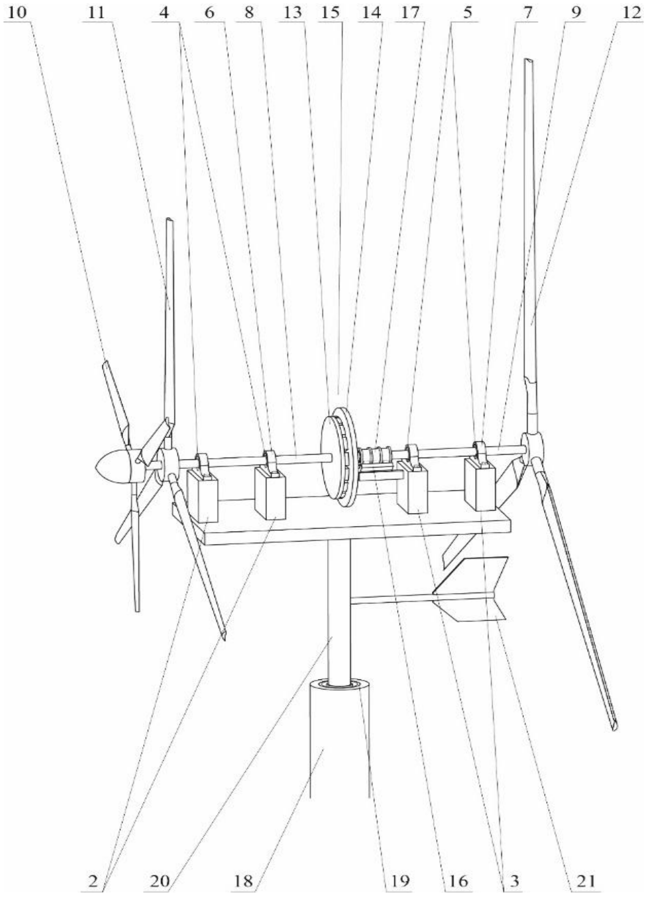

Figure 1. The structural schematic and kinematic arrangement of the proposed horizontal-axis wind turbine system

Figure 1 presents the structural schematic and kinematic arrangement of the proposed horizontal-axis wind turbine system. These parameters include the following:
(1 – nacelle casing; 2, 3 – metal structural supports; 4, 5 – mechanical bearings; 6, 7 – bearing housings/pedestals; 8 – primary drive shaft; 9 – secondary drive shaft; 10, 11 – front wind turbine rotors; 12 – rear wind turbine rotor; 13 – generator inductor; 14 – generator armature; 15 – three-phase electric generator; 16 – brush assembly; 17 – slip ring/collector; 18 – support tower; 19 – yaw bearing; 20 – metal tubular sleeve; 21 – passive aerodynamic yaw vane).

The proposed system consists of an aerodynamic nacelle (1) mounted onto a structural support tower (18) via a yaw bearing (19) and a vertical tubular sleeve (20). Directional orientation relative to incoming wind streamlines is passively maintained by an aerodynamic tail vane (21). The mechanical drive system comprises two independent, coaxially aligned rotating shafts:

Primary Counter-Clockwise Assembly: Two aerodynamic turbine rotors (10 and 11) having operational radii R_1 and R_2 ($R_1 < R_2$) are coaxially mounted at a fixed axial distance d along the primary drive shaft (8). The shaft (8) is supported on bearing housings (6) fitted with precision low-friction roller bearings (4), anchored rigidly to metallic base supports (2). Upon exposure to the incoming wind flow V_∞, this entire mechanical sub-assembly executes rotational motion in a counter-clockwise direction. The inner end of shaft (8) is firmly keyed to the outer inductor (13) of the coreless/synchronous generator (15).

Secondary Clockwise Assembly: The downstream wind turbine rotor (12) having an expanded operational radius R_3 ($R_3 > R_2$)is keyed to the secondary shaft (9). Shaft (9) is supported by bearing blocks (7) and bearings (5) fastened to rear metal supports (3). The aerodynamic pitch and camber of the blades of rotor (12) are engineered to drive shaft (9) in a clockwise direction. Shaft (9) is mechanically coupled to the inner armature (14) of the generator (15).

During system operation, kinetic energy extracted from the air flow across turbine rotors (10, 11, and 12) is converted into simultaneous, counter-directional rotational mechanical energy on shafts (8) and (9). Consequently, the generator inductor (13) and armature (14) rotate relative to one another at an effective angular velocity $w_{rel}=w_1+w_2$. This counter-rotating electromagnetic topology induces three-phase alternating current (AC) at significantly lower absolute rotor velocities, overcoming the typical cut-in limitations of conventional micro-scale wind turbines. The electrical power generated in the rotating armature (14) is routed through three-phase internal cabling connected to a rotating brush holder (16) mounted on shaft (9). Current is transmitted across stationary slip rings/commutators (17) securely fixed to the support structure (3), where it is subsequently delivered via low-loss transmission lines to the load controller or energy storage battery bank.

3. Mathematical Modeling and Aerodynamic Formulations

To evaluate the operational efficiency and aerodynamic energy conversion mechanism of the multi-rotor configuration, a staged 1D theoretical flow model based on momentum theory and static pressure discontinuities was formulated.

3.1. Mass Conservation and Continuity

The performance parameters of the proposed wind energy system are determined below. According to Fig. 7, the mass balance equation of the wind flow passing through the wind turbines of radii R_1 and R_2 positioned at a distance d from each other is expressed as follows:

$$\dot{m}_1 = \dot{m}_2 = \rho \cdot V_\infty \cdot (1 - a_1) \cdot A_1 = \rho \cdot V_\infty \cdot (1 - a_2) \cdot A_2 \quad (1)$$

$$A_1 = \pi \cdot R_1^2, \qquad A_2 = \pi \cdot R_2^2$$

where the swept circular frontal areas are defined as:

where: $\dot{m}_1$ and $\dot{m}_2$ − are the mass flow rates of the air stream; ρ − is the air density; V_∞ − the free-stream wind velocity; a_1 and a_2 − are the axial induction factors representing the wind velocity variations across the cross-sectional planes of the wind turbines; A_1 and A_2 −are the cross-sectional swept areas of the wind turbines.

To determine the ratio of the cross-sectional swept areas of the wind turbines with radii R_1 and R_2, the coefficient α_s introduced:

$$\alpha_s = \frac{A_1}{A_2} = \frac{R_1^2}{R_2^2} = \frac{(1-a_1)}{(1-a_2)} \quad (2)$$

Here, $0 < \alpha_s \leq 1$ present the axial induction factors expressing fractional wind velocity deceleration at the respective rotor planes.

The rate of change of momentum of the air stream flowing through the cross-sectional swept areas of the wind turbines with radii R_1 and R_2 can be expressed as follows:

$$\Delta P_1 \cdot A_1 + \Delta P_2 \cdot A_2 = \dot{m}_2 \cdot [V_\infty - V_\infty \cdot (1 - b_2)] \quad (3)$$

where: $\Delta P_1 = P_1 - P_1'$ and $\Delta P_2 = P_2 - P_2'$ are the static pressure differences generated across the upstream and downstream faces of the wind turbine rotors, respectively; b_1 and b_2 are the induction factors characterizing the wind flow velocity variations in the wake region surrounding the wind turbines.

By simplifying Equations (1) and (3), the following mathematical expression is derived:

$$\Delta P_1 \cdot A_1 + \Delta P_2 \cdot A_2 = \rho \cdot V_\infty^2 \cdot (1 - a_1) \cdot b_1 = \rho \cdot V_\infty^2 \cdot (1 - a_2) \cdot b_2 \quad (4)$$

Based on Bernoulli's principle, the static pressure differences of the airflow across the cross-sectional planes of the wind turbines with radii R_1 and R_2 are derived. These expressions are defined as follows:

Based on Bernoulli's principle, the static pressure differences of the airflow across the cross-sectional planes of the wind turbines with radii R_1 and R_2 are derived. These expressions are defined as follows:

$$P_\infty + \frac{\rho \cdot V_\infty^2}{2} = P_1 + \frac{\rho \cdot V_\infty^2}{2} \cdot (1 - a_1)^2 \quad (5)$$

$$P_1 + \frac{\rho \cdot V_\infty^2}{2} \cdot (1 - a_1)^2 = P_2 + \frac{\rho \cdot V_\infty^2}{2} \cdot (1 - a_2)^2 \quad (6)$$

ISSN NO: 2770-4491
June 2026

$$P_2 + \frac{\rho \cdot V_\infty^2}{2} \cdot (1 - a_2)^2 = P_\infty + \frac{\rho \cdot V_\infty^2}{2} \cdot (1 - b_2)^2 \quad (7)$$

From Equations (5)–(7), the following equation is obtained to relate the pressure drops across the wind turbines:

$$\Delta P_1 + \Delta P_2 = \frac{\rho \cdot V_\infty^2}{2} \cdot (1 - b_2) \cdot b_2 \quad (8)$$

Equation (22) reveals the dependence of the aerodynamic power coefficient C_p on the axial induction factor a_1, the downstream wake velocity deficit b_2, and the rotor cross-sectional area ratio α_s. Computational fluid dynamics (CFD) simulations performed in Ansys Fluent utilizing the shear stress transport (SST) k-w turbulence model were carried out to evaluate flow characteristics, blade surface pressure distributions, and inter-rotor wake dynamics.

Parametric sweeps of the induction factors demonstrate that the maximum aerodynamic power coefficient is attained at:

$$a_1 = 0;\ b_2 = 0{,}836 \text{ va } \alpha_s = 0{,}582$$

Substituting these optimal parameters into Equation (22):

$$C_p = 0.836 \cdot (2\text{-}0.836) \cdot (1\text{-}0) \cdot 0.582 + 16/27 \cdot (1\text{-}0.582) = 0.814$$

The maximum theoretical power coefficient achieved by the proposed three-rotor configuration is $C_p = 0.814$. This value represents a 37.3% enhancement over the classical single-rotor Betz limit$C_{pBetz} = 0.593$).

The physical mechanism underpinning this performance enhancement is two-fold:

1. The forward rotor pair (R_1 and R_2) decelerates the incoming flow while establishing a favorable radial pressure gradient that channels bypassing fluid toward the larger periphery of the rear rotor (R_3).
2. The counter-directional rotation of the rear turbine rotor (12) actively cancels tangential swirl velocities imparted to the wake, thereby recuperating rotational kinetic energy that is conventionally lost to the environment.

Determination of Optimal Axial Separation Distance (d)

The axial spacing distance d between the upstream rotor planes R_1 and R_2 plays a critical role in mitigating adverse aerodynamic blade-vortex interactions. If the distance d is too narrow, severe aerodynamic shadowing and boundary-layer interference suppress lift production on the second rotor. Conversely, excessive axial spacing increases cantilever bending moments on shaft (8), inducing dynamic vibration and nacelle mass penalties.

3. Result and Discussion

In this study, an innovative multi-rotor horizontal-axis wind turbine installation was designed, mathematically formulated, and aerodynamically characterized for decentralized power generation in low-wind-speed environments:

1. The structural integration of two forward co-rotating rotors (R_1, R_2) and one rear counter-rotating rotor (R_3) coupled directly to the inductor and armature of a three-phase generator doubles relative rotational speeds, obviating the need for mechanical gearboxes and lowering the cut-in wind speed threshold.
2. A modified 1D momentum mathematical model was established, providing analytical formulations for static pressure drops, thrust forces, and total power extraction across sequential rotor discs.
3. Numerical investigation conducted in Ansys Fluent established that for an optimal swept area ratio $\alpha_s = 0{,}582$, $a_1 = 0$, and wake deficit coefficient $b_2 = 0.836$, the maximum aerodynamic power coefficient reaches $C_p = 0.814$. This represents a 37.3% efficiency improvement over the theoretical single-rotor Betz limit.
4. The optimal axial separation between the forward rotor planes was determined to be $d = 0.1 \cdot R_2$, ensuring favorable aerodynamic interaction and structural stability.

The proposed three-rotor counter-rotating system provides a highly efficient, compact, and reliable technological solution for autonomous low-capacity consumers and off-grid renewable micro-grids.

Reference

ISSN NO: 2770-4491
June 2026

1. Vasel-Be-Hagh, A., Archer, C. L. "Counter-rotating vertical-axis and horizontal-axis wind turbines: A review of performance and aerodynamics." Renewable and Sustainable Energy Reviews, 2017, Vol. 77, pp. 627–643. https://doi.org/10.1016/j.rser.2017.03.111
2. Shen, X., Zhu, X., Du, Z. "Wind turbine aerodynamics and performance enhancement via multi-rotor and counter-rotating concepts: A comprehensive review." Energy Conversion and Management, 2021, Vol. 245, 114578. https://doi.org/10.1016/j.enconman.2021.114578
3. Rosenberg, A., Selvaraj, O., Sharma, A. "A novel dual-rotor turbine concept for increasing wind farm power density." Journal of Physics: Conference Series, 2014, Vol. 524, 012099. https://doi.org/10.1088/1742-6596/524/1/012099
4. Habash, R. W. Y., Groza, V. Z., Yang, P. "Performance evaluation of a small horizontal-axis counter-rotating dual-rotor wind turbine." IEEE Transactions on Sustainable Energy, 2011, Vol. 2, No. 4, pp. 407–414. https://doi.org/10.1109/TSTE.2011.2158450
5. Wang, L., Liu, X., Kolios, A. "State-of-the-art review on aerodynamics and design optimization of multi-rotor and counter-rotating wind turbines." Applied Energy, 2022, Vol. 308, 118337. https://doi.org/10.1016/j.apenergy.2021.118337